INTERNATIONAL JOURNAL FOR NUMERICAL METHODS IN FLUIDS, VOL. 23, 1223–1233 (1996)

NUMERICAL STUDY OF TURBULENT FORCED CONVECTION IN A PERIODICALLY RIBBED CHANNEL WITH OSCILLATORY THROUGHFLOW

TORU FUSEGI

Engineering Systems International/Nihon ESI K.K., 2-47-18 Uehara, Shibuya, Tokyo 151, Japan

SUMMARY

Numerical computations are performed on the fully developed flow and heat transfer in a periodically ribbed channel with oscillatory throughflow. A uniform heat flux is imposed at the lower plate of the channel. An externally sustained pressure gradient varies sinusoidally in time. A low-turbulent-Reynolds-number version of the k–ε two-equation model of turbulence is invoked, together with a preferential dissipation modification, to predict the complex turbulent flow field. Computed results indicate that much heat transfer enhancement is expected by increasing the Womersley number, which measures the relative strength of the oscillatory motion to the viscous effects.

KEY WORDS: finite difference method; heat transfer augmentation; eddy viscosity model; low-*Re* k–ε model; streamline curvature correction; ribbed channel

1. INTRODUCTION

Turbulent heat transfer in a channel with rib-roughened walls is of much engineering relevance. It is known to be an effective means of heat transfer enhancement in compact heat exchangers, cooling of electronic devices and other types of thermal engineering equipment. A higher heat transfer rate may be expected by imposing on the channel an externally sustained oscillatory pressure gradient, by which better mixing of the medium can be accomplished. It is thought to be a promising technique for cooling high-density electronic circuit boards, for which an excessively high flow rate of the cooling agent is not desirable from a mechanical design point of view. Despite its potential for innovative engineering applications, the available information on turbulent heat transfer in oscillatory flow is limited.

Ohmi *et al.*[1] measured the velocity profiles of oscillatory throughflow in a rectangular duct using hot-wire anemometry. Instantaneous velocity profiles for turbulent oscillatory flow were found to be similar to those of non-oscillatory flow. Consequently, the profiles contained little phase shift, contrasting with their laminar flow counterparts. The same authors have also constructed a flow regime diagram, thereby identifying the role of the mechanically imposed frequency (characterized by the Womersley number) in the flow transition. Their experiments were conducted under an isothermal condition.

Features of the flow field and mass transfer rate were investigated for a wavy walled channel by Nishimura *et al.*[2] With a smoothly contoured wall, flow separation and subsequent growth of a vortex, which eventually occupied the entire flow passage, were clearly observable in the acceleration stage. In the deceleration stage accompanying the reversal in the flow direction, these vortices were

CCC 0271–2091/96/111223–11

Received July 1995
Revised February 1996

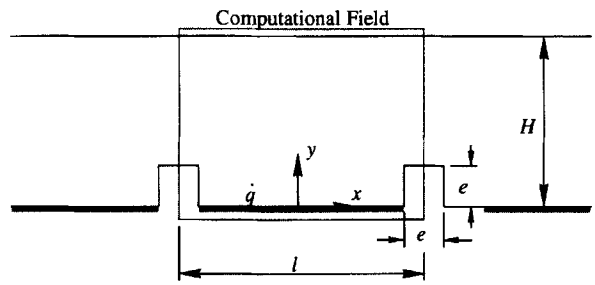

Figure 1. Geometry of problem the superscript '*' denoting dimensional quantities is omitted for brevity

seen to be ejected from the wall, followed by a quick entrainment of the throughflow to the cavity. The mass transfer rate was found to be much enhanced by the vortex dynamics compared with the case of a straight channel.

No prior computational work on turbulent oscillatory flow in a rib-roughened channel appears to exist in the open literature. In the present investigation, numerical computations are performed for the fully developed flow and heat transfer in a periodically ribbed channel with oscillatory throughflow. A low- turbulent-Reynolds-number amendment to the k–ε two-equation model of turbulence is made, together with a preferential dissipation modification to account for the streamline curvature effect. These enable one to capture the salient features of the flow field structure with a moderate increase in the complexity of the turbulence model and computational effort. A schematic diagram of the problem geometry is depicted in Figure 1. In the computations the flow field spanning the unit length of periodicity l is dealt with. Square ribs, measuring $e \times e$, are mounted on the lower wall of the channel. The inter-rib distance $L\ (=l-e)$ is heated by a constant heat flux $\dot{q}$. The pressure gradient across the channel varies sinusoidally as a function of time t. Of particular interest in the present study is the case in which there is no net mass flow per cycle of oscillations. Two values of the rib pitch Pi are assigned for the computations: $Pi=5$ and 7·2.

In the non-oscillatory flow regime a significant rise in the heat transfer rate took place for $Pi \approx 7$. The reattaching throughflow to the heated portion of the ribbed wall appearing at around this Pi was thought to be responsible for the heat transfer augmentation.[3] Once this occurred, the average Nusselt number increased only slightly even if Pi was increased. For lower Pi ($\leqslant 5$) there was little exchange of the mass of fluid between the cavity (the flow field between two adjacent ribs) and the throughflow; in this case a cavity-wide vortex was generated. Formation of such a flow structure prevented the throughflow from contacting the heated surface directly.

In the present study the effects of externally imposed oscillatory pressure gradients on the heat transfer rate are examined for the two exemplary rib pitches.

MATHEMATICAL MODEL

Two-dimensional (in the mean quantities) incompressible fluid flow is assumed. Furthermore, the physical properties of the fluid (with $Pr=0{\cdot}7$) are assumed to be constant.

The first step towards deriving the proper working equations is to filter out turbulent fluctuations from the original time-dependent governing equations that describe completely the instantaneous fields (the Navier–Stokes equations) through an appropriate time-averaging process. Namely, time averaging is applied to any physical quantity ϕ as

$$\bar{\phi} = \frac{1}{\Delta t}\int_{\tau-\Delta t/2}^{\tau+\Delta t/2} \phi \, \mathrm{d}t,$$

where τ in this expression is a dummy variable of integration. A time interval Δt is chosen in such a manner that it may remove turbulent fluctuations effectively without affecting the oscillatory components imposed externally on the throughflow. This procedure, called *short-time averaging*, makes sense as long as a characteristic wave number of random turbulent fluctuations composed of high modal frequencies is sufficiently different from that of the forced oscillations in the throughflow (possessing a low modal frequency).

Referring to the co-ordinate system depicted in Figure 1, the fully developed flow and heat transfer in a two-dimensional channel may be conveniently described by the short-time-averaged governing equations

$$\frac{\partial \bar{u}}{\partial x}+\frac{\partial \bar{v}}{\partial y}=0, \tag{1}$$

$$\frac{Wo^2}{Re}\frac{\partial \bar{u}}{\partial t}+\frac{\partial \bar{u}^2}{\partial x}+\frac{\partial \bar{v}\bar{u}}{\partial y}=-\frac{\partial \bar{p}}{\partial x}+\frac{Wo^2}{Re}\cos t+\frac{1}{Re}\left[\frac{\partial}{\partial x}\left(\nu_{\text{eff}}\frac{\partial \bar{u}}{\partial x}\right)+\frac{\partial}{\partial y}\left(\nu_{\text{eff}}\frac{\partial \bar{u}}{\partial y}\right)\right], \tag{2}$$

$$\frac{Wo^2}{Re}\frac{\partial \bar{v}}{\partial t}+\frac{\partial \bar{u}\bar{v}}{\partial x}+\frac{\partial \bar{v}^2}{\partial y}=-\frac{\partial \bar{p}}{\partial y}+\frac{1}{Re}\left[\frac{\partial}{\partial x}\left(\nu_{\text{eff}}\frac{\partial \bar{v}}{\partial x}\right)+\frac{\partial}{\partial y}\left(\nu_{\text{eff}}\frac{\partial \bar{v}}{\partial y}\right)\right], \tag{3}$$

$$\frac{Wo^2}{Re}\frac{\partial \bar{\theta}}{\partial t}+\frac{\partial \bar{u}\bar{\theta}}{\partial x}+\frac{\partial \bar{v}\bar{\theta}}{\partial y}+\bar{u}\Theta=\frac{1}{Re}\left[\frac{\partial}{\partial x}\left(\alpha_{\text{eff}}\frac{\partial \bar{\theta}}{\partial x}\right)+\frac{\partial}{\partial y}\left(\alpha_{\text{eff}}\frac{\partial \bar{\theta}}{\partial y}\right)\right], \tag{4}$$

where

$$\nu_{\text{eff}}=1+\nu_{\text{t}}, \qquad \alpha_{\text{eff}}=\frac{1}{Pr}+\frac{\nu_{\text{t}}}{Pr_{\text{t}}}, \qquad \nu_{\text{t}}=C_\mu f_\mu Re\frac{k^2}{\varepsilon}.$$

These expressions may be reached from the short-time-averaged equations by splitting the pressure $\bar{P}$ and temperature $\bar{T}$ into periodic components ($\bar{p}$ and θ) and non-periodic (linear) parts,[4]

$$\bar{P}^*=\bar{p}^*-\rho\Pi\cos(\omega t^*)x^*, \qquad \bar{T}^*=\bar{\theta}^*+\Theta^* x^*, \tag{5}$$

and subsequently non-dimensionalizing the resulting equations according to the manner explained in the Appendix. As the second term on the right-hand side of the above equation for pressure indicates, the pressure gradient is assumed to vary as a cosine function of time. Furthermore, from the energy balance at a given time it can be seen that

$$\Theta^*=\dot{q}L^*/l^* c_{\text{p}}(\dot{m}(t^*))^* \quad (\text{for} \quad \dot{m}^*\neq 0).$$

Since the mass flow rate has one-to-one correspondence with the pressure gradient in a given physical condition, Θ^* is an implicit function of time. The special case $\dot{m}^*=0$ leads to an infinite value of Θ^*; however, this is not a problem in a discrete system, since the proper arrangement of t^* can avoid the occurrence of a singularity in the numerical computation.

These mean flow equations are complemented by the k–ε model equations

$$\frac{Wo^2}{Re}\frac{\partial k}{\partial t}+\frac{\partial \bar{u}k}{\partial x}+\frac{\partial \bar{v}k}{\partial y}=\frac{1}{Re}\left[\frac{\partial}{\partial x}\left(\nu_{k,\text{eff}}\frac{\partial k}{\partial x}\right)+\frac{\partial}{\partial y}\left(\nu_{k,\text{eff}}\frac{\partial k}{\partial y}\right)\right]+P_k-\varepsilon, \tag{7}$$

$$\frac{Wo^2}{Re}\frac{\partial \varepsilon}{\partial t}+\frac{\partial \bar{u}\varepsilon}{\partial x}+\frac{\partial \bar{v}\varepsilon}{\partial y}=\frac{1}{Re}\left[\frac{\partial}{\partial x}\left(\nu_{\varepsilon,\text{eff}}\frac{\partial \varepsilon}{\partial x}\right)+\frac{\partial}{\partial y}\left(\nu_{\varepsilon,\text{eff}}\frac{\partial \varepsilon}{\partial y}\right)\right]+\frac{\varepsilon}{k}(C_{\varepsilon 1}P_\varepsilon-C_{\varepsilon 2}f_\varepsilon\varepsilon), \tag{8}$$

where

$$P_k = \frac{\nu_t}{Re}\left[2\left(\frac{\partial \bar{u}}{\partial x}\right)^2 + 2\left(\frac{\partial \bar{v}}{\partial y}\right)^2 + \left(\frac{\partial \bar{u}}{\partial y} + \frac{\partial \bar{v}}{\partial x}\right)^2\right], \qquad \nu_{k,\text{eff}} = 1 + \frac{\nu_t}{Pr_k}, \qquad \nu_{\varepsilon,\text{eff}} = 1 + \frac{\nu_t}{Pr_\varepsilon}.$$

A low-turbulent-Reynolds-number k–ε model proposed by Abe *et al.*[5] is employed in the present investigation. In this model the wall-damping effect of turbulence is measured by the Kolmogorov velocity scale u_ε ($u_\varepsilon^* \equiv (\nu\varepsilon^*)^{1/4}$), thereby making the model applicable to flows with separation. The model functions f_μ and f_ε contained in the above equations are given[5] as

$$f_\mu = \left[1 - \exp\left(-\frac{\Delta}{14}\right)\right]^2 \left\{1 + \frac{5}{R_t^{3/4}} \exp\left[-\left(\frac{R_t}{200}\right)^2\right]\right\},$$
$$f_\varepsilon = \left[1 - \exp\left(-\frac{\Delta}{3{\cdot}1}\right)\right]^2 \left\{1 - 0{\cdot}3 \exp\left[-\left(\frac{R_t}{6{\cdot}5}\right)^2\right]\right\}, \tag{9}$$

where $\Delta \equiv (u_\varepsilon^* \Delta^*)/\nu$, Δ being the nearest distance from a wall, and $R_t \equiv Re\ k^2/\varepsilon$.

A word is in order regarding the source term P_ε, the production of turbulent kinetic energy by strain, in the ε-equation. In the original formulation[5] this term is equal to P_k appearing in the k-equation, i.e. $P_\varepsilon - P_k$. Note that in the present problem the fluid passes through a succession of flow contractions formed by the ribs. As a result, flows experience strong acceleration in a periodic fashion. The original model is unable to cope with this situation and numerical stability arises. A compensation for streamline curvature correction, termed PDM (preferential dissipation modification),[6] is a remedy for such circumstances. Within the framework of PDM an expression for P_ε effective for recirculating flow is

$$C_{\varepsilon 1} P_\varepsilon = C_{\varepsilon 11} P_k - C_{\varepsilon 12} \nu_t S_{ns}^2, \tag{10}$$

where S_{ns} is the shear strain in the direction of the streamline, which may be computed from a formula given in Reference 6. The constants $C_{\varepsilon 1}$, $C_{\varepsilon 11}$ and $C_{\varepsilon 12}$ are related as $C_{\varepsilon 1} = C_{\varepsilon 11} - C_{\varepsilon 12}$. Furthermore, it was found[3] that for non-oscillatory flows in a ribbed channel the model constants have to be slightly altered from the original values[5] to lead the calculation to closer agreement with existing experimental and numerical data. The results are summarized in Table I. These values are adopted in the present investigation for an oscillatory flow system.

Table I. Turbulence model constants[3]

	C_μ	$C_{\varepsilon 1}$	$C_{\varepsilon 11}$	$C_{\varepsilon 12}$	$C_{\varepsilon 2}$	Pr_t	Pr_k	Pr_ε
$Pi > 5$	0·09	1·5	2·3	0·8	1·9	0·7	1·4	1·4
$Pi \leqslant 5$	0·09	1·56	2·36	0·8	1·9	0·7	1·6	1·6
Unribbed[a]	0·09	1·5	—	—	1·9	0·7	1·4	1·4

[a] PDM is not used.

The pertinent boundary conditions are

$$\begin{aligned}
&\bar{u} = \bar{v} = k = 0 \quad \text{at the solid wall (no-slip condition),}\\
&\varepsilon = \frac{2}{Re}\left(\frac{\partial\sqrt{k}}{\partial n}\right)^2, \quad \text{the normal derivative at the solid wall,}\\
&\partial\bar{\theta}/\partial y = 1 \quad \text{in} \quad -L/2 \leqslant x \leqslant L/2 \quad \text{at} \quad y = 0 \quad \text{(uniform heat flux),}\\
&\partial\bar{\theta}/\partial n = 0, \quad \text{the normal derivative at the other walls (insulated wall),}\\
&(\bar{u}, \bar{v}, \bar{p}, \bar{\theta}, k, \varepsilon)|_{x=l/2} = (\bar{u}, \bar{v}, \bar{p}, \bar{\theta}, k, \varepsilon)|_{x=-l/2} \quad \text{(periodic condition).}
\end{aligned} \tag{11}$$

SOLUTION METHOD

The governing equations (1)–(4), (7) and (8) together with the appropriate boundary conditions (11) are solved numerically using the finite volume method. A non-staggered grid arrangement is employed for discretization of the Navier–Stokes equations. Consequently, all the dependent variables are stored at the cell centres. The specific procedure employed for collocating grid points is PWIMC (pressure-weighted interpolation method corrected).[7] A novel feature of PWIMC lies in the way it evaluates the velocities at the control volume faces: they are interpolated with appropriate weighting from the adjacent cell centre velocities. This assures the coupling of the velocity fields to the pressure field and effectively eliminates non-physical wiggles of pressure.[8] For more complete information on PWIMC the reader should consult the cited literature.[7] Aside from the non-staggered grid approach that replaces the standard staggered grid methodology, the present iterative solution technique follows the well-known SIMPLE algorithm.[8]

The spatial derivatives are approximated by central differences of second-order accuracy, except for the convection terms for which the third-order QUICK upwind scheme[9] is applied. The Euler backward difference formula is utilized for integration in time. The finite difference equations are solved sequentially by applying cylic TDMA,[4] which is particularly suited for a periodic computational domain.

In order to accelerate convergence, a multigrid method based on an additive correction strategy[10] is utilized for solving the finite difference equations.

Convergence at any time step is declared when the following criterion is met:

$$|\phi^n - \phi^{n-1}|/|\phi^n|_{\max} \leqslant 10^{-5} \quad \text{for all grid points and all variables,} \tag{12}$$

where ϕ denotes a dependent variable. The superscripts n and $n-1$ refer to the current and previous iteration levels respectively.

The majority of the computations are conducted using grids of 61×61 (for $Pi = 5$) and 81×61 (for $Pi = 7{\cdot}2$) points. The meshes are non-uniformly spaced to sufficiently resolve the spatial resolution for steep gradients of the variables near the solid walls. Grid dependence of the solutions has been assessed for non-oscillatory flows in a straight (unribbed) channel and a ribbed channel.[3] The time step increment is set to $\Delta t = 0{\cdot}025\pi$ ($\Delta\tau = 1/80$) to secure time-step-independent solutions.

Code validation

The developed solution procedure for turbulent oscillatory flows has been validated through comparison with existing experimental data. For an unribbed channel, measurements were taken for the fully developed flow under an isothermal condition[1] and for the mass transfer rate.[2] They serve as reference data for code validation.

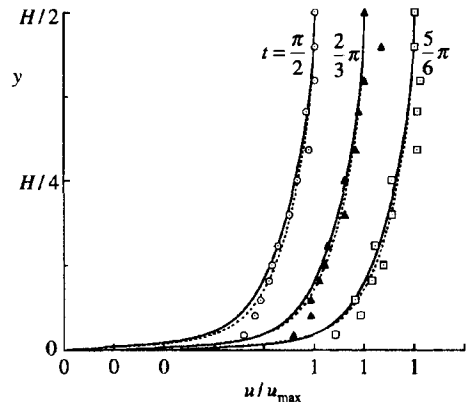

Figure 2. Velocity profiles normalized with respect to maximum values u_{max} at three phase angles of oscillations (t) for a straight channel ($Re = 6 \times 10^4$): ——, oscillatory flow; ·····, non-oscillatory flow; symbols, experimental results of Ohmi *et al.*[1]

The profiles of the u-velocity up to the centreline of the channel ($y = H/2$) at three different phase angles of oscillations are depicted in Figure 2, together with laser velocimetry measurements[1] and the computed profiles for non-oscillatory throughflow. At the given oscillatory Reynolds number Re of 6×10^4 the positive-half-cycle-averaged mean velocity $\langle u_m \rangle$ and the maximum centreline velocity u_{max} are found to be 0·436 and 0·757 respectively. These translate into a peak-velocity-based Reynolds number Re_u of $4{\cdot}54 \times 10^4$. The Womersley number is set to $Wo = 20$. These measurements[1] were conducted at $Re_u = 3{\cdot}39 \times 10^4$ and $Wo = 20{\cdot}4$. When normalized by the centreline velocity, these profiles are similar and close to the u-velocity distribution for a non-oscillatory channel at the corresponding Re_u, as noted by Ohmi *et al.*[1] The experimental data[1] exhibit significant scattering over the entire height of the channel. The computed velocity profiles may be roughly regarded as least-square-fitted curves for these data points, except near the wall, where taking accurate measurements would be difficult. Overall, the present numerical predictions are seen to be consistent with these experimental results.

The heat or mass transfer rate can serve as an indicator of changes in the varaibles in the close proximity of the wall. Measurements were taken for the mass transfer rate using an electrochemical method[2] at an St_u ($= Wo^2/Re_u$) of 0·0432. Secured date were compiled in terms of $Sh_{av}/Sc^{1/3}$, where Sh_{av} and Sc are the average Sherwood number and the Schmidt number respectively. The present computation, in which the lower wall of the channel is heated over the entire length (i.e. $L = l$), is performed for $Re = 3 \times 10^4$ and $Wo = 40$, giving $Re_u = 3{\cdot}4 \times 10^4$ and $St_u = 0{\cdot}047$. The computed heat transfer rate is $Nu_{av}/Pr^{1/3} = 53{\cdot}0$ (with $Pr = 0{\cdot}7$). Assuming the analogy between heat and mass transfer, this compares well with $Sh_{av}/Sc^{1/3} = 58$ cited in the literature.[2]

RESULTS AND DISCUSSION

The computations are performed for $Re = 2 \times 10^4$ and $40 \leqslant Wo \leqslant 160$ (i.e. $0{\cdot}08 \leqslant St \leqslant 1{\cdot}28$). In all cases, periodic states are reached after two or three cycles of oscillations, irrespective of arbitrarily prescribed initial guesses. The results pertaining to these periodic states, which are independent of initial conditions, are presented in this section.

Since the flow field in the vicinity of the ribs, especially that between two adjacent ribs, has a significant bearing on the heat transfer process at the lower wall of the channel, a detailed examination of the flow features in the channel is undertaken. For illustrative purposes, Figure 3

reproduces short-time-averaged streamlines at selected phase angles τ in one cycle of oscillations at $Wo = 80$ and $Pi = 7{\cdot}2$. Changes in the size and shape of the recirculating cell formed near the upstream corner of the rib are of much interest. A circulatory cell is present near the upstream corner of the rib in Figure 3(a). In the acceleration stage ($\dot{m}$ increasing) this vortex convects slightly downstream, as seen in Figure 3(b), for which $\dot{m}$ is close to its peak value. Weak corner vortices are discernible near the ribs in the same figure. In the deceleration stage the aforementioned circulatory cell grows in size and eventually extends over the entire area formed between the ribs (Figure 3(c)). However, when $\dot{m}$ further decreases and approaches zero, the throughflow starts to penetrate into the inter-rib zone, responding to a considerable reduction in the overall intensity of the flow. (This gives rise to an increase in the heat transfer rate due to the sweeping action of the throughflow over the heated surface, as observable in Figure 4). In Figure 3(d), in which the direction of the throughflow has reversed, the streamlines in the throughflow are appreciably curved. Also seen in this figure is the formation of a distinctive secondary cell near the new upstream corner of the rib. This flow field is

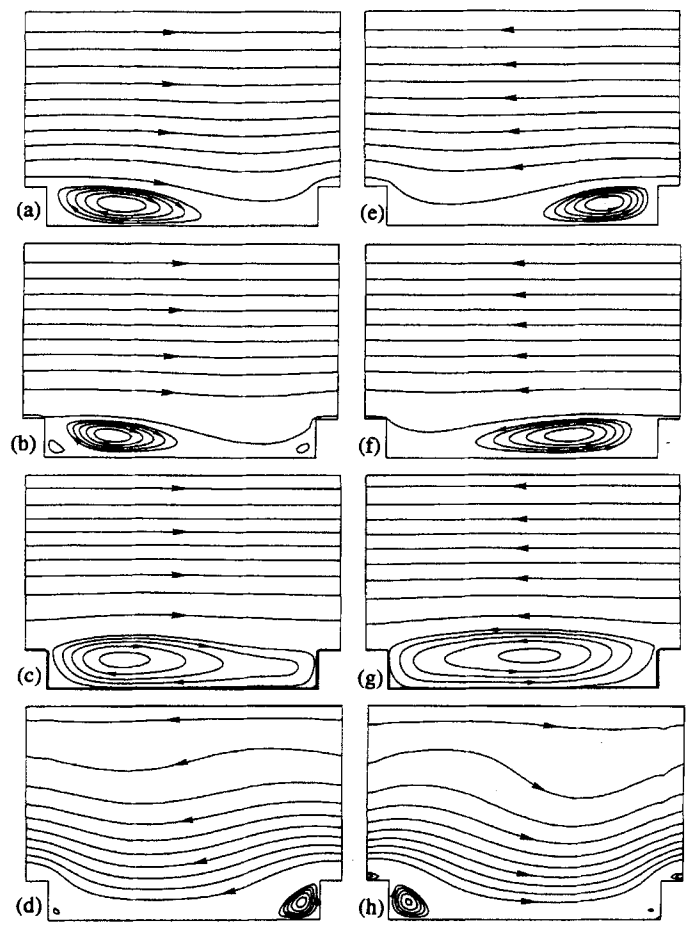

Figure 3. Short-time-averaged streamlines ($Re = 2 \times 10^4$, $Wo = 80$, $Pi = 7{\cdot}2$): (a) $\tau = 1/8$ ($\Delta\bar{\psi} = 0{\cdot}065$ (throughflow) and $2{\cdot}8 \times 10^{-3}$ (recirculating cell), $\dot{m} = 0{\cdot}667$); (b) $\tau = 1/4$ ($\Delta\bar{\psi} = 0{\cdot}079$ and 2×10^{-3}, $\dot{m} = 0{\cdot}773$); (c) $\tau = 3/8$ ($\Delta\bar{\psi} = 0{\cdot}047$ and $3{\cdot}4 \times 10^{-3}$, $\dot{m} = 0{\cdot}418$); (d) $\tau = 1/2$ ($\Delta\bar{\psi} = 0{\cdot}018$ and 8×10^{-4}, $\dot{m} = -0{\cdot}201$); (e) $\tau = 5/8$ ($\Delta\bar{\psi} = 0{\cdot}067$ and $2{\cdot}2 \times 10^{-3}$, $\dot{m} = -0{\cdot}679$); (f) $\tau = 2/3$ ($\Delta\bar{\psi} = 0{\cdot}08$ and 2×10^{-3}, $\dot{m} = -0{\cdot}782$); (g) $\tau = 7/8$ ($\Delta\bar{\psi} = 0{\cdot}05$ and 5×10^{-3}, $\dot{m} = -0{\cdot}442$); (h) $\tau = 1$ ($\Delta\bar{\psi} = 0{\cdot}015$ and 10^{-3}, $\dot{m} = 0{\cdot}184$)

now in the new acceleration stage ($\dot{m}$ towards its minimum). In Figures 3(e)–3(h) the flow patterns are closely antisymmetric with respect to those of the corresponding τs presented in Figures 3(a)–3(d).

It deserves mention that the flow features at $Pi = 5$ (not shown) are qualitatively similar to those at $Pi = 7{\cdot}2$ examined above. In the non-oscillatory flow cases they differ noticeably: the secondary cell spans the entire cavity at $Pi = 5$, while the flow separation and subsequent reattachment take place at $Pi = 7{\cdot}2$ near the downstream corner.[3] For achieving a high heat transfer rate, the latter flow pattern is favourable, since the fluid is thought to be better mixed. In the oscillatory flow system it may be of interest to inspect the effect of Pi over a wide range to identify the extent of Pi for which this flow structure is maintained; however, this is left for future work owing to the large computational effort necessary for turbulent oscillatory flow calculations.

In Figure 4, time histories of the $\bar{u}$-velocity at $(x, y) = (0, 0{\cdot}25)$, the mass flow rate across the channel ($\dot{m}$) and the average Nusselt number at the heated wall (Nu_{av}) are plotted over the four cycles of oscillations. The periodic nature of the flow is apparent. It should be noted that the changes in these quantities lag behind the variation in the imposed pressure gradient possessing cosine function form, $\cos t$. The local velocity $\bar{u}$ and $\dot{m}$ are seen to be in phase.

A comprehensive description of the flow and heat transfer characteristics is provided in Figure 5, in which the positive-half-cycle-averaged mass flow rate $\langle \dot{m} \rangle$ and Nusselt number $\langle Nu_{av} \rangle$ are displayed as functions of Wo for the two rib pitches. For comparison purposes, results of the unribbed channel ($Pi = 0$) and non-oscillatory flow system ($Re_m = 2 \times 10^4$, $Wo = 0$) are also plotted in these figures. The straight lines connecting these data points are drawn only for the sake of understanding trends. The computed average Nusselt numbers (Nu_{av}) for the non-oscillatory flow are in excellent agreement with the available measurements.[11,12] For the oscillatory flow, much heat transfer enhancement takes place upon increasing Wo at $Pi = 7{\cdot}2$. A noteworthy feature of the unribbed channel is the laminarization of the flow at high Wo. This results in a noticeable decrease in $\langle Nu_{av} \rangle$. In

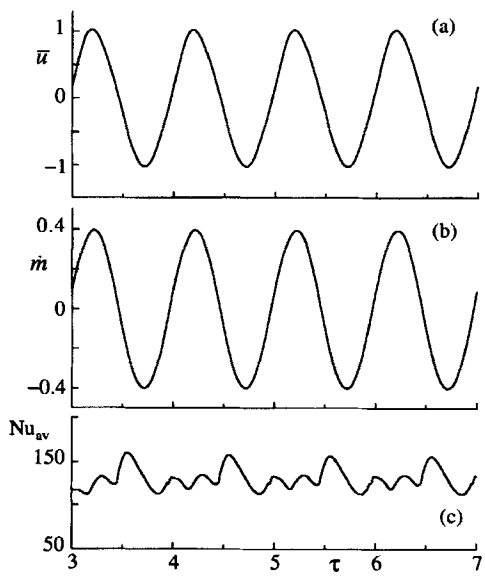

Figure 4. Time histories of (a) local velocity at centre of flow field ($(x, y) = (0, 0{\cdot}25)$), $\bar{u}$, (b) mass flow rate through channel, $\dot{m}$, and (c) average Nusselt number at heated wall, Nu_{av} ($Re = 2 \times 10^4$, $Wo = 80$, $Pi = 7{\cdot}2$)

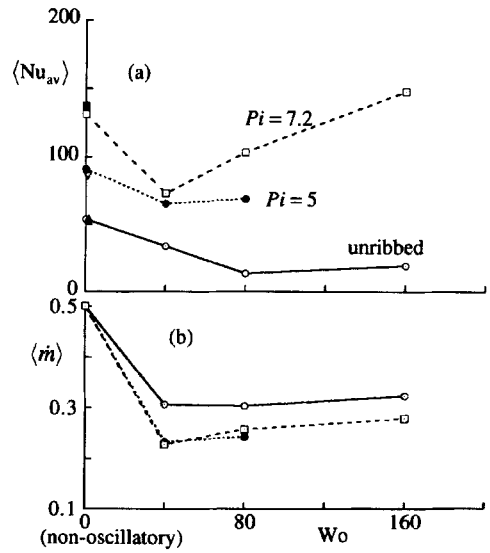

Figure 5. Positive-half-cycle-averaged Nusselt number $\langle Nu_{av} \rangle$ and mass flow rate $\langle \dot{m} \rangle$ as functions of Womersley number Wo ($Re = 2 \times 10^4$): ■, Reference 11; ▽ and ▲, Reference 12; other plots, present computational results

this figure the average Nusselt number attainable using high-Wo oscillatory flows in a rib-roughened channel (with zero net flow rate) is generally comparable with that of the non-oscillatory flow with much higher uniform flow rate.

CONCLUSIONS

The detailed structure of the fully developed flow field in a periodically ribbed channel subjected to oscillatory throughflow is studied numerically. To construct the numerical solution procedure, a recently proposed low-turbulent-Re k–ε model[5] is employed, together with the preferential dissipation modification scheme[6] to handle strong streamline curvature effects.

The developed numerical model has been validated against the available experimental data for oscillatory channel flows.[1,2] The computed results for the ribbed channel demonstrate that the imposed oscillatory pressure gradient causes marked variations in the transient features of the flow field, especially in the inter-rib zone. Furthermore, it has been confirmed that the eminent vortical structure has significant bearing on the heat transfer rate at the constant-heat-transfer surface at the lower wall of the channel. Heat transfer is found to be enhanced as the throughflow sweeps directly over the heated surface. As the relative importance of oscillatory components becomes more pronounced with an increase in Wo, heat transfer augmentation is expected with little change in the mass flow rate of the throughflow over the parameter ranges investigated in the present study. Heat transfer using oscillatory flow may be regarded as a high-performance cooling technology in various thermal engineering applications.

APPENDIX: NOMENCLATURE

c_p	specific heat at constant pressure (J kg^{-1} K^{-1})
$C_{\varepsilon 1}$, $C_{\varepsilon 2}$, C_μ	turbulence model constants
D_H	hydraulic diameter of channel ($=2H$) (m)

e	rib height, e^*/D_H
f_ε, f_μ	turbulence model functions (defined by equation (9))
H	unobstructed channel height, H^*/D_H
k	turbulent kinetic energy, $k^*/(\Pi/\omega)^2$
l	length of periodicity of channel, l^*/D_H
L	heated length, L^*/D_H
$\dot{m}$	mass flow rate per unit span, $\dot{m}^*/\rho(\Pi/\omega)D_H$
Nu	local Nusselt number, $\dot{q}D_H/\lambda(\theta_w^* - \theta_b^*)$
Nu_{av}	average Nusselt number, $(1/L)\int_{-L/2}^{L/2} Nu\ \mathrm{d}x$
$\bar{p}$	short-time-averaged pressure, $(\bar{p}^* - \frac{2}{3}\rho k^* - p_h)/\rho(\Pi/\omega)^2$, p_h being the hydrostatic pressure (N m^{-2})
Pi	rib pitch, l/e
Pr, Pr_t	molecular and turbulent Prandtl numbers
$\dot{q}$	heat flux (W m^{-2})
R_t	turbulent Reynolds number
Re	oscillatory flow Reynolds number, $(\Pi/\omega)D_H/\nu$
Re_m	mass-flow-rate-based Reynolds number, $\langle\dot{m}^*\rangle/\rho\nu$ $(=\langle\dot{m}\rangle Re)$
Re_u	Reynolds number based on maximum velocity at centreline of channel, $u_{max}\|_{y=H/2}D_H/\nu$ $(= Re_m u_{max}\|_{y=H/2}/\langle u_m\rangle$, where u_m is the mean velocity)
St	Strouhal number $(= Wo^2/Re)$
t	time, ωt^*
$\bar{u}, \bar{v}$	short-time-averaged velocity components in directions x and y, $(\bar{u}^*, \bar{v}^*)\omega/\Pi$
Wo	Womersley number, $D_H\sqrt{(\omega/\nu)}$
x, y	Cartesian co-ordinates, $(x^*, y^*)/D_H$

Greek letters

α	thermal diffusivity (ms^{-2})
ε	dissipation rate of k, $\varepsilon^* D_H/(\Pi/\omega)^3$
$\bar{\theta}$	short-time-averaged temperature, $\bar{\theta}^*\lambda/\dot{q}D_H$
θ_b	bulk temperature, $\int_0^H \|\bar{u}\|\theta\mathrm{d}y/\int_0^H \|\bar{u}\|\mathrm{d}y$
Θ	parameter defined by equation (5), $\Theta^*\lambda/\dot{q}$
λ	thermal conductivity of fluid (W m^{-1} K^{-1})
ν	molecular viscosity (m^2 s^{-1})
ν_t	eddy viscosity, ν_t^*/ν
Π	parameter defined by equation (5) (m s^{-2})
ρ	density (kg m^{-3})
τ	normalized time, $t/2\pi$
$\bar{\psi}$	short-time-averaged streamfunction, $\bar{\psi}^*/D_H(\Pi/\omega)$
ω	frequency of oscillations (s^{-1})

Subscripts

eff	effective diffusivity
w	at the wall

Superscript

*	dimensional quantity

Miscellaneous

$\overline{(\ )}$ short-time-averaged (see text for definition)

$\langle \cdot \rangle$ positive-half-cycle-averaged, $(1/\pi)\int_0^{2\pi} \max[\cdot, 0]\, dt$ ($\max[a, b]$ denotes the larger of the two arguments)

REFERENCES

1. M. Ohmi, M. Iguchi and F. Akao, 'Laminar–turbulent transition and velocity profiles in rectangular duct for oscillatory flow', *Trans. JSME B*, **49**, 2343–2353 (1983).
2. T. Nishimura, A. Tarumoto and Y. Kawamura, 'Flow and heat transfer characteristics in wavy channels for oscillatory flow', *Int. J. Heat Mass Transfer*, **30**, 1007–1015 (1987).
3. T. Fusegi, 'Turbulent flow calculations of mixed convection in a periodically-ribbed channel', *J. Enhanced Heat Transfer*, **2**, 295–305 (1995).
4. S. V. Patankar, C. H. Liu and E. M. Sparrow, 'Fully developed flow and heat transfer in ducts having streamwise-periodic variations of cross-sectional area', *J. Heat Transfer*, **99**, 180–186 (1977).
5. K. Abe, T. Kondoh and Y. Nagano, 'A new turbulence model for predicting fluid flow and heat transfer in separating and reattaching flows— I. Flow field calculations', *Int. J. Heat Mass Transfer*, **37**, 139–151 (1994).
6. M. A. Leschziner and W. Rodi, 'Calculation of annular and twin parallel jets using various discretization schemes and turbulence-model variations', *J. Fluids Eng.*, **103**, 352–360 (1981).
7. M. H. Kobayashi and J. C. F. Pereira, 'Calculation of incompressible laminar flows on a nonstaggered, nonorthogonal grid', *Numer. Heat Transfer B*, **19**, 243–262 (1991).
8. S. V. Patankar, *Numerical Heat Transfer and Fluid Flow*, Hemisphere, Washington, DC, 1980.
9. B. P. Leonard, 'A stable and accurate convective modelling procedure based on quadratic upstream interpolation', *Comput. Methods Appl. Mech. Eng.*, **19**, 59–98 (1979).
10. B. R. Hutchinson and G. D. Raithby, 'A multigrid method based on the additive correction strategy', *Numer. Heat Transfer*, **9**, 511– 537 (1986).
11. J. F. Lockett, 'Heat transfer from roughened surfaces using laser interferometry', *Ph.D. Thesis*, Department of Mechanical Engineering, City University, London, 1987.
12. J. C. Han, L. R. Glicksman and W. M. Rohsenow, 'An investigation of heat transfer and friction for rib-roughened surfaces', *Int. J. Heat Mass Transfer*, **21**, 1143–1156 (1978).